

Why Are Halo Density Profiles Stable at Formation?

Guillermo González-Casado

Departamento de Matemática Aplicada II, Universidad Politécnica de Cataluña, Pau Gargallo 5, 08028 Barcelona, Spain

Andreu Raig and Eduard Salvador-Solé

Departamento de Astronomía y Meteorología, Universidad de Barcelona, Av. Diagonal 647, 08028 Barcelona, Spain

Abstract. We analyze the physical justification of the picture proposed by Salvador-Solé et al. in these proceedings for the time evolution of the universal density profile of dark-matter halos. According to this picture, halos have at formation a stable (i.e. independent of mass and time) dimensionless density profile, the characteristic length and density scales of the profile depending on the underlying cosmogony. Subsequent evolution is driven by mass accretion onto the outskirts of halos and can be characterized simply by the increment of halo radius with time and the corresponding decrease of the critical density of the universe. We find this picture to be a reasonable good description of the expected evolution of halos in hierarchical models of structure formation.

1. Introduction

Relying on data from high resolution N-body simulations performed by Navarro, Frenk & White (1997, NFW), Salvador-Solé et al. (1998, S98) derived the laws for the evolution of the dimensionless characteristic length and density scales (x_s and δ_c respectively) of the universal density profile of dark-matter halos proposed by NFW. For a halo of mass M at time t (redshift z), those laws have the following expressions:

$$x_s(t, M) = x_{sf} \frac{R(t_f)}{R(t)}, \quad (1)$$

$$\delta_c(z, M) = \delta_{cf} \frac{\Omega(z)(1+z_f)}{\Omega(z_f)(1+z)}, \quad (2)$$

where $R(t)$ is the virial halo radius at t , $\Omega(z)$ is the cosmic density at z in units of the critical density of the universe (ρ_{crit}), and t_f and z_f are the formation time and formation redshift of the halo, respectively. It is important to remark that equations (1) and (2) are two independent fitting formulae. N-body simulations show that x_s and δ_c are, in fact, linked through the condition that the mean internal density of halos within the virial radius is equal to about $200\rho_{\text{crit}}$ (implying that halo density profiles are one-parametric functions). Equations (1)

and (2) are found to be consistent with that property for different cosmological models (cf. S98).

It is evident that the proportionality constants x_{sf} and δ_{cf} (which are cosmogony dependent) correspond to the values of x_{s} and δ_{c} when halos form, respectively. Therefore, the values of the scale radius, $r_{\text{s}} = x_{\text{s}}R(t)$, and of the characteristic density, $\rho_{\text{c}} = \delta_{\text{c}}\rho_{\text{crit}}(z)$, of halo density profiles are set at the halo formation time. Halo formation is basically characterized by the last major merger yielding a substantial re-arrangement of the internal structure of merging halos (see Salvador-Solé et al. in these proceedings for a quantitative definition). After formation, subsequent evolution by matter accretion (secondary infall and/or minor mergers) does not change the values of r_{s} and ρ_{c} . However, since $\rho_{\text{crit}}(z)$ decreases with time while $R(t)$ increases accordingly, the values of x_{s} and δ_{c} change as described by equations (1) and (2).

In the present work we develop a physical model with the aim of checking the validity of the picture proposed for the evolution of the scaling parameters of halo density profiles. On the other hand, we will try to determine for a set of cosmogonies analyzed the corresponding shape of the stable density profile of halos at their formation time.

2. The Structure of Halos Formed by Binary Major Mergers

In this section we describe the model linking the scaling parameters of the density profile of new formed halos and their progenitors. Let us assume that halos form essentially through the major merger of two halo progenitors (this approach is justified in the next section). In practice, as a major merger we mean that if a halo has a formation mass M_0 , then its two halo progenitors have masses M_1 and M_2 (with $M_1 \geq M_2$) so that $M_2/M_1 > \Delta_m = 0.6$. The threshold Δ_m between major and minor mergers is an empirical parameter introduced to allow for a better motivated definition of the formation time of halos. The value of $\Delta_m = 0.6$ has been derived by fitting the mass-density correlation of halos in high resolution N-body simulations (see S98).

Consider a halo of mass M_0 with internal energy U_0 at its formation time, t_f , and the system formed by its two halo progenitors at the time they reach turnaround. The total energy of the system at turnaround can be written as:

$$E_{\text{ta}} = U_1 + U_2 + E_{12}, \quad (3)$$

where U_i is equal to the sum of the internal energy of the virialized mass of the i -th halo progenitor at turnaround plus the total energy of the mass that will be accreted onto that halo from turnaround until t_f . The last term in the right-hand-side of equation (3) gives the mutual gravitational interaction plus orbital kinetic energy of the system at turnaround.

If there is not significant mass-loss neither during the formation process of M_0 , nor during mass accretion onto halo progenitors from turnaround until t_f , then from energy conservation one has

$$U_0 = U_1 + U_2 + E_{12}, \quad (4)$$

and also for $i = 1, 2$ one can approximate U_i by the internal energy of halo progenitors at t_f . Therefore, for $i = 0, 1, 2$ one can write

$$U_i = -\frac{1}{2} \frac{GM_i^2}{R_i} F(x_{si}), \quad (5)$$

where M_i and R_i are the mass and the radius of each halo at t_f , respectively, and $M_1 + M_2 = M_0$. In writing equation (5) it has been assumed that halos are virialized systems described by a universal density profile, which determines the specific expression of function $F(x_s)$.

Concerning the expression of E_{12} , it can be written as

$$E_{12} = \left[\frac{S}{2(1 - M_2/M_1)} - 1 \right] \frac{GM_1 M_2}{D_m}, \quad (6)$$

where D_m is the turnaround separation between halo-progenitor centers. In the well known point-mass approximation and taking t_f equal to one orbital period one gets:

$$D_m^3 = (2 - S)^3 GM_0 \left(\frac{t_f}{2\pi} \right)^2. \quad (7)$$

The so-called circularity parameter, S , appearing in equations (6) and (7) takes into account that halo progenitors can merge following a non-radial orbit. For an elliptical orbit of eccentricity e , one has $S = 1 - e$. Thus, a radial orbit corresponds to $S = 0$ while a circular orbit to $S = 1$. For an object moving in an arbitrary orbit of total energy E one has $S = J^2/J_c^2(E)$ (Merritt 1985), where J is the angular momentum of the orbit and $J_c(E)$ is the angular momentum of a circular orbit of energy E . Non-radial mergers are caused by external torques from the large-scale matter distribution surrounding halo progenitors. In hierarchical structure formation scenarios one expects that low-mass halos will merge in non-radial orbits while massive halos will tend to merge in nearly radial orbits. On the other hand, the mutual tidal interaction between merging halos slows-down the orbital motion and the final merger time will be longer than the value computed for point masses (eq. [7]). In practice, this can be accounted for by assuming a non-null value of S , which for a fixed D_m increases t_f by a certain amount. The larger the mass of merging halos the stronger the expected effect of mutual tides on the merger time. Therefore, the combined action of external torques and mutual tides between halo progenitors can be described by a value of S different from zero for a wide mass range. The exact mass dependence of S is difficult to predict, but in a first approximation the influence of both external torques and mutual tides on the final results can be addressed by taking a constant value of S over the whole mass range analyzed.

Substituting equations (5), (6), and (7) into equation (4) one derives the following equation:

$$\begin{aligned} F(x_{sf}) &= \left(\frac{M_1}{M} \right)^{\frac{5}{3}} F(x_{s1}) + \left(\frac{M_2}{M} \right)^{\frac{5}{3}} F(x_{s2}) \\ &+ (2 - S)^{-1} \left[1 - \frac{S}{2(1 - M_2/M_1)} \right] \left(\frac{\pi}{5\tau} \right)^{\frac{2}{3}} \frac{M_1 M_2}{M^2}, \end{aligned} \quad (8)$$

where $\tau = t_f H(t_f)$ and $H(t)$ is the Hubble parameter at t . In the left-hand-side of equation (8) we have written x_{sf} instead of x_{s0} because the latter corresponds to the value of the dimensionless scale radius of M_0 at its formation time. The expression of $F(x_s)$ for spherically symmetric halos in hydrostatic equilibrium with an isotropic velocity distribution is completely determined by the halo density profile, $\rho(r)$, which is assumed universal. The different shapes for that universal profile considered in the present work are particular cases of the following general expression (Zhao 1996)

$$\rho(r) = \frac{\rho_c}{y^\alpha (1 + y^\beta)^{\frac{\gamma-\alpha}{\beta}}}, \quad (9)$$

where $y = r/r_s$ and r is the radial distance to the halo center. From this density profile one can infer the corresponding mass profile $M(r)$, the one-dimensional velocity dispersion profile $\sigma(r)$, and finally, one can compute $F(x_s)$ from the following expression:

$$F(x_s) = -\frac{U}{GM^2/(2R)} = \frac{c}{[m(c)]^2} \left[\int_0^c m(y) \hat{\rho}(y) y \, dx - c^3 \hat{\rho}(c) \hat{\sigma}^2(c) \right], \quad (10)$$

where $\hat{\rho}(y) = \rho(r)/\rho_c$, $m(y) = M(r)/(4\pi r_s^3 \rho_c)$, $\hat{\sigma}(y) = \sigma(r)/\sqrt{4\pi G r_s^2 \rho_c}$, and $c = x_s^{-1}$ is the halo concentration parameter.

To sum up, we detail the steps followed by the practical implementation of the present model:

Step 1: Starting from a halo of mass M at a fixed time t , we compute by means of the S98 clustering model the halo formation time t_f , its formation mass M_0 , the typical mass of its halo progenitors, M_1 and M_2 , and the formation time of the latter, t_{f1} and t_{f2} .

Step 2: An empirical value of the dimensionless scale radius (denoted by x_{sf}^e) is assumed for halo progenitors of any mass at their formation time. This is equivalent to setting a stable density profile at formation for all progenitors considered if a universal halo density profile is assumed.

Step 3: The value of x_{sf}^e is evolved from the formation time of each halo progenitor t_{fi} till their merger time corresponding to the formation time t_f of the resulting new halo M_0 . This yields the dimensionless scale radii for the density profile of halo progenitors, x_{s1} and x_{s2} , at time t_f that will be inserted into equation (8). The evolution of x_{sf}^e can be computed from either equation (1) or equation (2). We have checked that both yield consistent results to within typically 10%.

Step 4: Solving equation (8) for x_{sf} we derive the theoretical dimensionless scale radius for the density profile of M_0 at formation (denoted by x_{sf}^t) which has to be compared with the corresponding empirical value assigned to halo progenitors in step 2, x_{sf}^e .

3. Progenitor Masses and Binary Major Mergers

As stated at the beginning of the previous section, we assume that major mergers tracing the formation of new halos are essentially binary. This can be justified in the framework of the clustering model developed by S98.

Consider a halo of mass M_1 that incorporates a certain amount of mass ΔM at time t . According to S98, if $\Delta M/M_1 > \Delta_m$ then M_1 is destroyed and a new halo of mass $M_0 = M_1 + \Delta M$ is formed by a major merger, while if $\Delta M/M_1 \leq \Delta_m$ the halo $M_0 = M_1 + \Delta M$ is the result of the evolution of the halo M_1 by mass accretion and/or minor mergers, hence M_1 is not destroyed, it simply changes its mass to M_0 .

Now assume that, in the case of major mergers, the mass ΔM always comes from a single halo that hereafter we denote by M_2 . It is easy to see that

$$\frac{\Delta_m M_0}{1 + \Delta_m} < M_i < \frac{M_0}{1 + \Delta_m}, \quad \text{for } i = 1, 2. \quad (11)$$

This interval limiting the mass of halo progenitors is centered at $M_0/2$, and $|M_1 - M_0/2| = |M_2 - M_0/2|$, or equivalently, M_1 and M_2 are at the same distance of $M_0/2$. Therefore, the distribution function of halo progenitor masses should be a symmetric function around $M_0/2$. This distribution function can be derived from the S98 clustering model and, hence, its symmetry can be checked (see Raig et al. 1998). We find that indeed the symmetry is fulfilled to within 3% and this result is independent of redshift and of the cosmogony considered. The symmetry of the distribution function of halo progenitors strongly supports that major mergers are essentially binary.

4. Results

In this section we will present the results of the comparison between the dimensionless scale radius at formation for halos of mass M and their progenitors (x_{sf}^t and x_{sf}^e respectively), according to the model described in §2. This comparison will be performed for different cosmogonies and a fixed universal density law of the form given by NFW. Subsequently, we will consider the implications of assuming a different universal density profile. The set of cosmogonies analyzed in the present work is described in columns (1) to (5) of Table 1. We have considered a standard biased cold dark matter model (SCDM), a flat cold dark matter model with non-null cosmological constant (Λ CDM), and a power-law model with power index $n = -1$ and flat geometry. These models were also analyzed by NFW and S98. In Table 1, Ω_0 is the matter density parameter, Λ_0 is the cosmological constant in units of $3H_0^2$, where $H_0 = 100 h \text{ km s}^{-1} \text{ Mpc}^{-1}$, and σ_8 is the rms mass fluctuation in spheres of radius $8 h^{-1} \text{ Mpc}$.

In Figures 1 and 2 we show the fractional difference between x_{sf}^t and x_{sf}^e for the SCDM and the Λ CDM models, respectively, assuming a universal NFW density profile. Similar curves are found for the power-law model. Results are plotted as a function of halo masses at $z = 0$ scaled to the characteristic mass M_* defining a unity rms density fluctuation. For cosmogonies which are self-similar or close to self-similar the results expressed in this way are redshift independent. Thick solid lines correspond to different values of the parameter S and were derived assuming a value of x_{sf}^e equal to the best fit dimensionless scale radius found by S98 from their analysis of the NFW N-body simulations. The concrete values are shown in column (7) of Table 1, and in column (8) are listed the 90% confidence intervals resulting from the χ -square fit.

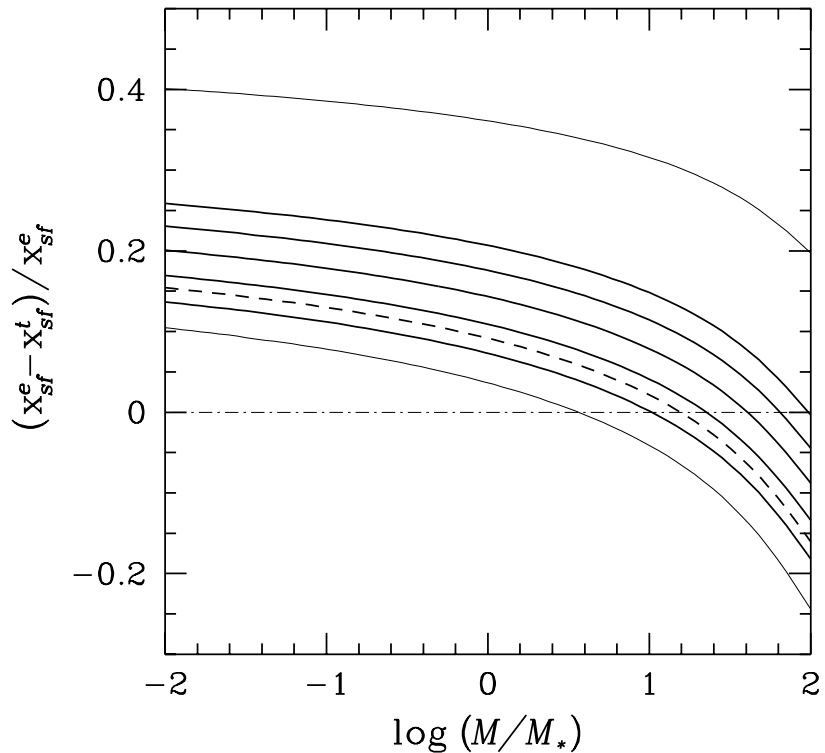


Figure 1. Fractional difference between the dimensionless scale radius at formation for halos of mass M and their progenitors (x_{sf}^t and x_{sf}^e respectively) in the case of an SCDM cosmology and assuming an NFW universal density law for dark-matter halos. The different thick solid lines correspond to different values of the parameter S ranging from $S = 0$ (upper curve) to $S = 1$ (lower curve) in steps of 0.25. They were derived by taking x_{sf}^e equal to the best fit value obtained in S98 (see Table 1). Thin solid lines correspond to twice (upper) and half (lower) the latter value for $S = 0$. Finally, the thick dashed line has been derived for the value of x_{sf}^e that minimizes the maximum fractional difference in the whole mass range (denoted as x_{sf}^m in the text). The shape of this latter curve is independent of the value of S assumed.

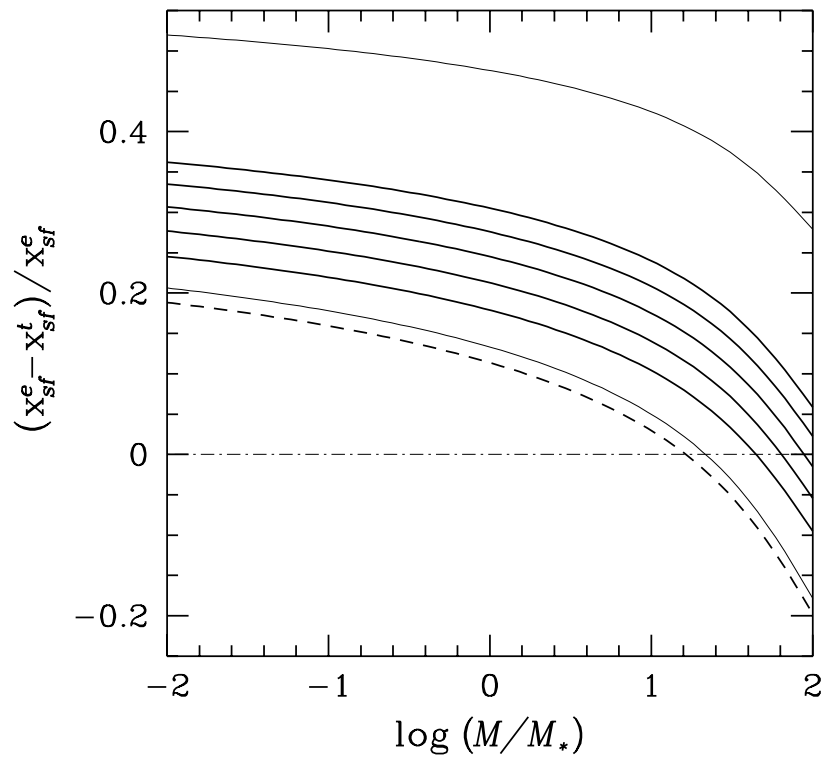


Figure 2. Same as Fig. 1 but for the Λ CDM model.

As can be seen from Figures 1 and 2 the fractional difference is not far from zero as expected if the dimensionless scale radius of halos were nearly fixed at formation. It is important to notice that taking into account the dynamical effects of external torques and mutual tides ($S > 0$) tends to improve the consistency with a universal value of x_{sf} . The maximum fractional difference is typically between 20% and 35% and is found for low-mass halos. For massive halos the agreement is quite satisfactory. On the other hand, another interesting result is that our model can be used to predict the value of x_{sf}^e which is in better agreement with the stability of halo density profiles at formation. As we show in Figures 1 and 2 (upper and lower thin solid lines), a significant change in the value of x_{sf}^e leads to a significant variation in the resulting fractional error. Consequently, we have derived the value of x_{sf}^e that minimizes the maximum fractional difference in the whole mass range analyzed. The results, denoted by x_{sf}^m , are shown in column (6) of Table 1 for the case of $S = 0.5$, an intermediate value of the circularity parameter. The corresponding fractional error curve in Figures 1 and 2 has been plotted as a thick dashed line. The values of x_{sf}^m are systematically smaller than the best fit values from S98 but always within the 90% confidence intervals from Table 1.

Table 1. Scaling of the NFW Density Law for Different Cosmogonies

$P(k)$ (1)	Ω_0 (2)	Λ_0 (3)	σ_8 (4)	h (5)	x_{sf}^m (6)	x_{sf}^* (7)	90% c.i. (8)
SCDM	1.0	0.0	0.63	0.5	0.14	0.17	(0.12,0.25)
Λ CDM	0.25	0.75	1.3	0.75	0.18	0.29	(0.18,0.52)
$n = -1.0$	1.0	0.0	1.0	0.5	0.10	0.17	(0.10,0.30)

* best fit value from S98

Recent N-body simulations by Moore et al. (1997) suggest a profile of different shape from the one advocated by NFW. This could rise the question whether our results do depend on the form of the universal law assumed to describe dark-matter halo density profiles. To clarify this point we have repeated the previous analysis for different universal halo density laws in addition to the NFW profile. The latter corresponds to $(\alpha, \beta, \gamma) = (1, 1, 3)$ in equation (9), while the rest of profiles considered are: the Hernquist (1990) law, $(\alpha, \beta, \gamma) = (1, 1, 4)$; the three-dimensional (3D) King law, $(\alpha, \beta, \gamma) = (0, 2, 3)$; and the profile proposed by Moore et al. (1997) to fit their high resolution N-body simulations, $(\alpha, \beta, \gamma) = (1.4, 1.4, 2.8)$. One can scale the values of x_s and δ_c from the NFW profile to the rest of density laws by assuming that the maximum in the different circular velocity profiles is at the same physical distance to halo center. The Hernquist and NFW profiles are similar in the innermost regions of halos. The Hernquist profile has a different slope from the NFW profile in the outermost regions of halos although it was found to provide a satisfactory fit to halo density profiles (NFW). On the other hand, in the outermost regions the NFW and the 3D King laws are similar. The 3D King law has a flat core which up to now has not been found in any cosmological N-body simulation (within the nominal resolution scale), but this profile provides a good description of the distribution

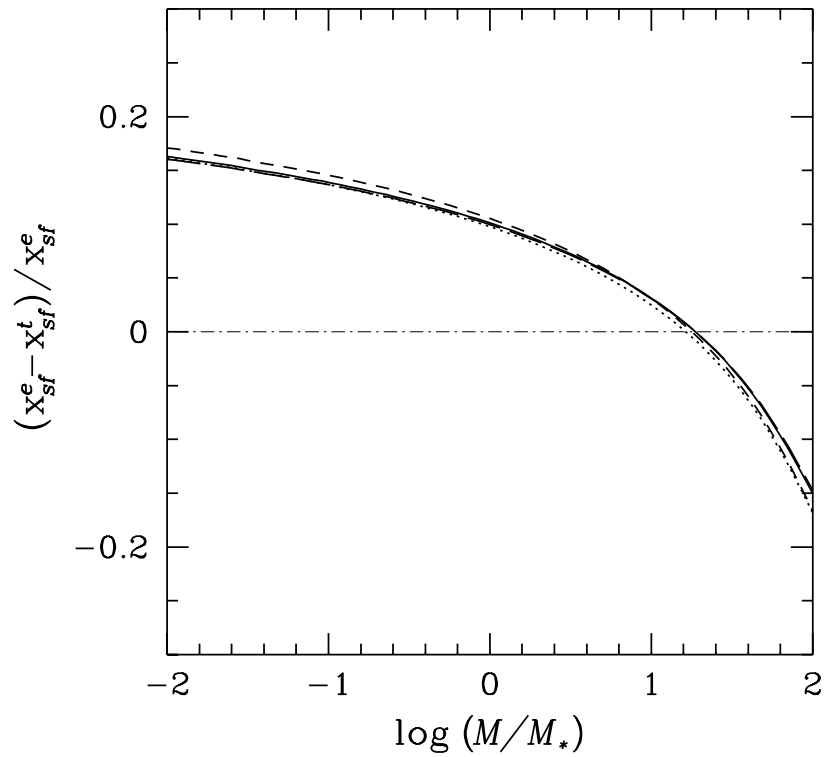


Figure 3. The best predictions of our model for the SCDM cosmogony in the case of the NFW density profile (solid line), the Hernquist profile (dotted line), the Moore et al. profile (short-dashed line), and the 3D King law (long-dashed line).

of galaxies in clusters. For the present study, the King law can be considered as providing a limiting case for the slope of the density profile in the central region of halos. Since the exact value of this slope is still a subject of debate, we have included in our study the profile suggested by Moore et al. (1997).

For each density profile we have derived the value of the dimensionless scale radius at formation that, according to our model, minimizes the maximum fractional difference between x_{sf}^e and x_{sf}^t in the mass range considered. As illustrated by Figure 3 corresponding to the Λ CDM cosmology, all density profiles lead to essentially the same result concerning the fractional difference. On the other hand, with respect to the value of x_{sf}^m inferred for the NFW profile, the values obtained for the other density laws analyzed differ in less than 20%.

5. Conclusions

The results of our study confirm the picture proposed in S98 and by Salvador-Solé et al. in these proceedings to describe the scaling evolution of universal halo density profiles. Halos form with a universal value of the dimensionless scale radius and scale density, x_{sf} and δ_{cf} , i.e., halos have stable density profiles at formation. Subsequently, halos evolve by accretion and the corresponding evolution of x_{s} and δ_{c} is well described by equations (1) and (2). Our study has covered a mass range of four decades, typically from the mass of galaxies to the mass of galaxy clusters. We have shown that the validity of the proposed picture is not affected by the specific form assumed for the universal density law of dark-matter halos. For density laws of the form (9) we always reach at essentially the same best model-predicted fractional difference between the values of x_{sf} for halo progenitors and the new halos they form. We have derived for different cosmologies the values of x_{sf} which lead to the best consistency with the previous picture. The resulting values are found to be in agreement with the best fit ones obtained by S98 from the analysis of N-body simulations.

According to the previous conclusions, in order to characterize the scaling evolution of halo density profiles, a first physical principle such as energy conservation during halo formation has to be taken into account. But at the same time, one also requires a clustering model properly describing halo formation and evolution through an adequate distinction between major mergers, tracing the formation of new objects, and minor mergers, corresponding to accretion onto otherwise relaxed halos. On the other hand, the exact form of the universal density profile of halos, which can not be determined by our analysis, would be set by more complicated processes than those included in the present study. Those processes would probably be linked to violent relaxation during halo formation in the framework of approximately self-similar cosmologies.

Acknowledgments. This work has been supported by the Dirección General de Investigación Científica y Técnica under contract PB96-0173 and by the Universidad Politécnica de Cataluña research project PR9707.

References

Hernquist, L. 1990, ApJ, 356, 359

- Merritt, D. 1985, *ApJ*, 289, 18
- Moore, B., Governato, F., Quinn, T., Stadel, J., & Lake, G. 1998, *ApJ*, 499, L5
- Navarro, J.F., Frenk, C.S., White, S.D.M. 1997, *ApJ*, 490, 493 (NFW)
- Raig, A., González-Casado, G., & Salvador-Solé, E. 1988, *ApJL*, in press (astro/ph 9810168)
- Salvador-Solé, E., Solanes, J.-M., & Manrique, A. 1998, *ApJ*, 499, 542 (S98)
- Zhao, H.S. 1996, *MNRAS*, 278, 488